Chinese Chemical Letters 35 (2024) 108862

Contents lists available at ScienceDirect

Chinese Chemical Letters

journal homepage: www.elsevier.com/locate/cclet

Development of functional dye with redshifted absorption based on Knoevenagel condensation at 1-site in phenyl[*b*]-fused BODIPY

Tianze Wang[a,1], Junyi Ren[b,1], Dongxiang Zhang[a,1], Huan Wang[b], Jianjun Du[c,*], Xin-Dong Jiang[a,*], Guiling Wang[b,*]

[a] *Liaoning & Shenyang Key Laboratory of Functional Dye and Pigment, Shenyang University of Chemical Technology, Shenyang 110142, China*
[b] *Department of Cell Biology, China Medical University, Shenyang 110122, China*
[c] *State Key Laboratory of Fine Chemicals, Dalian University of Technology, Dalian 116024, China*

ARTICLE INFO

Article history:
Received 10 April 2023
Revised 24 July 2023
Accepted 26 July 2023
Available online 28 July 2023

Keywords:
NIR dyes
[*b*]-Fused BODIPY
Knoevenagel condensation
Photothermal therapy
Cell apoptosis

ABSTRACT

Integrating ring-fused modification with π-conjugated extension is an effective approach for designing, synthesizing, and application for novel borondipyrromethene (BODIPY) structures. In this work, based on phenyl[*b*]-fused BODIPY, we made reasonable modification of the methyl group at 1-site to generate dye **NBDP**. **NBDP** possessed near-infrared region (NIR) absorption and emission properties, and the intramolecular charge transfer (ICT) resulted in low fluorescence. Whereas, heat energy is evidently released in the presence of light, which can be exploited for intracellular photothermal therapy *via* the cell apoptosis process, reducing the inflammatory side-effects induced by necrosis. This research provides a crucial foundation for the novel molecule *via* BODIPY multi-directional alteration and its potential application in anti-tumor phototherapy.

Aromatic [*b*]-fused modification in borondipyrromethene (BODIPY) system is remarkably advantageous for restraining the segment rotation to lead to dramatic spectroscopic bathochromic shift (Fig. 1a) [1–3]. BODIPY chromophore has the favorable light-stability and the excellent light absorption capacity [4–8]. Therefore, excellent photophysical properties of BODIPY allow it to be employed in fluorescence labeling [9–11], organic photoelectric materials [12,13], laser dyes [14,15], photodynamic therapeutic [16–19], photothermal therapy [20–22] and other innovative applications [23–25]. To achieve multi-site alteration for specific applications, it is critical to synthesize the BODIPY core from various structural platform.

Knoevenagel condensation with an aldehyde can be usually accomplished at 3,5-sites in BODIPY system (Fig. 1a), and the functional fragments can be linked by the olefinic bond [26–28]. And meanwhile, the spectral redshift and the π-conjugated structure extension are both achieved [29,30]. Absorption of red or near-infrared region (NIR) light, which is preferable for better tissue penetration and less background interference, is required for biomedicine [31–33]. Considering the cumulative effect of ring-fused configuration and Knoevenagel condensation, the BODIPY chromophore can be manipulated with 1,7,3,5-sites for extending absorption wavelength and integrating functional substituent such as dimethylamino group (-NMe_2) to promote intramolecular charge transfer (ICT) (Fig. 1a) [34,35]. In order to investigate and compare the utility, structural variations contribute to a specific application. For instance, by enhancing the radiation transition of $S_1 \rightarrow S_0$, dye provides an highly efficient fluorescence [36–38]. Inhibiting the radiation transition and boosting the non-radiation transition will contribute to the production of thermal energy for the treatment of cancer cells [39,40].

Recently, a strategy of the upper ring-fused configuration (Fig. 1a) and Knoevenagel condensation at 3,5-sites by our group was employed to provide NIR-absorbing dye [26]. However, Knoevenagel condensation of a methyl group at 1- or 7-site in BODIPY needs ingenious design to prohibit what happened at 3,5-sites (Fig. 1a). This phenyl[*b*]-fused strategy prevented 3,5-sites –CH_3 groups from participating in the condensation reaction, thus this condensation could only appear at 1,7-sites. Herein, we successfully constructed an underneath aromatic[*b*]-fused BODIPY dye, and established a dimethylaminophenyl connection at 1-site (Fig. 1b). However, we also attempted to develop bis-substituted derivative at 1,7-sites. Yet, the bis-substituted compounds were not obtained, because the activity of methyl groups at 1,7-sites was more inertial than that of 3,5-sites [5,24]. The ICT effect be-

* Corresponding authors.
E-mail addresses: dujj@dlut.edu.cn (J. Du), xdjiang@syuct.edu.cn (X.-D. Jiang), glingwang@cmu.edu.cn (G. Wang).
[1] These authors contributed equally to this work.

https://doi.org/10.1016/j.cclet.2023.108862
1001-8417/

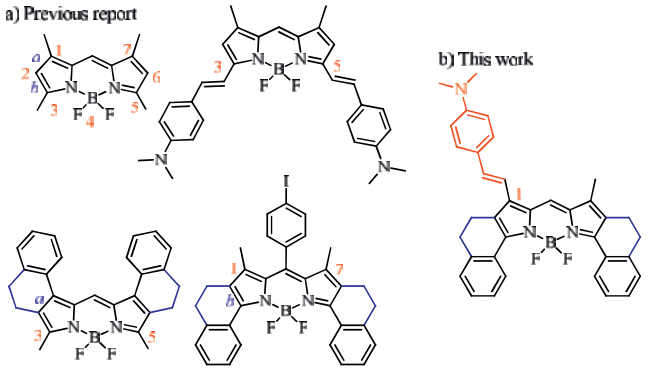

Fig. 1. (a) BODIPY generated by Knoevenagel condensation and aromatic[*b*]-fused BODIPYs. (b) Structure of BODIPY with a (*p*-NMe_2)styryl group at 1-site.

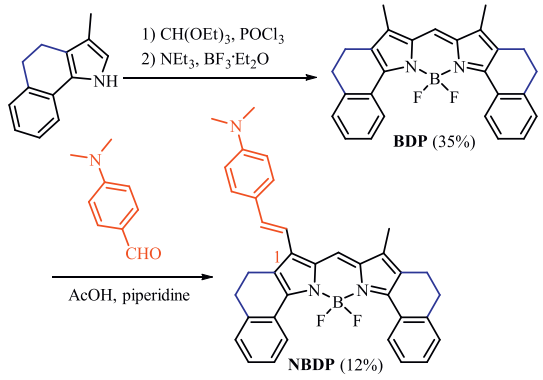

Scheme 1. Synthesis of **NBDP** generated by phenyl[*b*]-fused **BDP**.

tween the $-NMe_2$ group and the BODIPY core can significantly reduce fluorescence, and the results showed negligible photosensitive but improved photothermal capabilities, achieving photothermal conversion efficiency (PCE: 46.9%), and provided a remarkable killing function on light-activated cancer cells. These results of this research reveal innovative improvements to the BODIPY core, as well as an in-depth examination of its photophysical characteristics and photoinduced capacity for therapeutic strategies *via* cancer cells apoptosis pathway, blocking the development of inflammation [41,42]. This provides a valuable point of reference for the concept and application of innovative structure in BODIPY system.

Aromatic[*b*]-fused strategy in BODIPY system, not only takes advantage of prominent photophysical properties such as strong light capture ability, but also enhances photostability and π-extend conjugated structure, which is an appropriate modification approach. So, according to the new aromatic[*b*]-fused **BDP**, we conducted the olefinic interlinkage at 1-site *via* Knoevenagel condensation of dimethylaminobenzaldehyde to generate **NBDP** in 12% yields (Scheme 1). The structure of **NBDP** was confirmed by ^1H and ^{13}C nuclear magnetic resonance (NMR) spectroscopy as well as high resolution mass spectrometer (HRMS) (Figs. S1–S6 in Supporting information). As demonstrated in Fig. 2, the maximal absorption and emission of 674 and 742 nm were both located in the NIR spectrum. **NBDP** with dimethylaminophenyl group at 1-site displayed a dramatic redshift in absorption (110 nm) and emission (167 nm) in CH_2Cl_2, with high molar extinction coefficients (ε = 166,000 L mol^{-1} cm^{-1}), wide full width at half maximum (FWHM: 82 nm) and low fluorescence quantum yield ($\Phi_f = 0.02$), comparing to those of the parent dye **BDP** ($\lambda_{abs}/\lambda_{em}$ = 564/575 nm, ε = 145,000 L mol^{-1} cm^{-1}, $\Phi_f = 0.77$ and FWHM = 20 nm in CH_2Cl_2). The pictures of **BDP** (pink) and **NBDP** (green) in CH_2Cl_2 under normal conditions shows a vivid color difference (Fig. 2a).

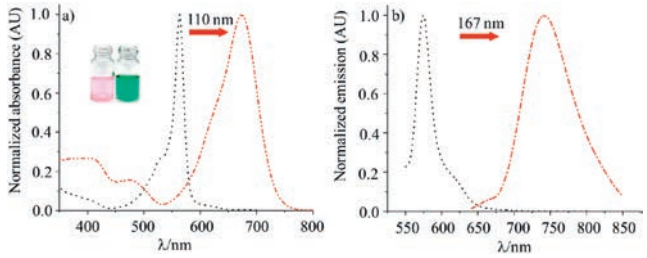

Fig. 2. (a) Normalized absorption and (b) fluorescence spectra of **BDP** (black) and **NBDP** (red) in CH_2Cl_2 at 298 K.

Additionally, absorption maxima of **NBDP** have little effects on different solvents, however the fluorescence quenching effect is more significant in large polar solvents such as *N*,*N*-dimethylformamide (DMF) and dimethyl sulfoxide (DMSO) owing to ICT (Fig. S7 and Table S1 in Supporting information). The highest occupied molecular orbital (HOMO) and the lowest unoccupied molecular orbital (LUMO) of the dyes were calculated by Gaussian 09 using the density functional theory (DFT) method. The HOMO level of **NBDP** was mostly distributed in the electron-donating dimethylamine phenyl group, whereas the LUMO level was primarily dispersed in the electron-deficient BODIPY center, establishing an electron donor-acceptor system. The energy level gaps between the HOMO and LUMO orbitals are also determined to be 2.468 and 2.128 eV of **BDP** and **NBDP**, respectively. This reduced energy of HOMO and LUMO orbital well explains the absorption redshift (Fig. 2a) by the condensed dimethylaminophenyl fragment (Fig. S8 in Supporting information).

To enable better applicability in physiological diagnostic and therapeutic applications, dye **NBDP** nanomaterials (**NBDP-**NPs) were further constructed with the amphiphilic polymer 1,2-distearoyl-*sn*–glycero-3-phosphoethanolamine-*N*-[methoxy(polyethylene glycol)–2000] ($DSPE\text{-}PEG_{2000}$). This boosted aqueous solubility and biocompatibility of **NBDP-**NPs. Dynamic light scattering (DLS) examination revealed the average hydrodynamic diameter of **NBDP-**NPs to be 75.23 nm, and the polymer dispersity index (PDI) to be 0.267, as depicted in Fig. 3a. Based on the transmission electron microscope (TEM) image, **NBDP-**NPs presents a spherical state with uniform size, which is conducive to further application in cells (Fig. 3b). Green **NBDP-**NPs in aqueous solution still indicated favorable distribution and stabilization after 7 days (Fig. 3c). The enhanced water solubility is beneficial to the application of biological samples.

The $^1O_2$ production capabilities of the **NBDP** was evaluated. To track the formation of $^1O_2$ while exposed to 690 nm laser radiation, 1,3-diphenylisobenzofuran (DPBF) was chosen as the sensor, because the absorbance of DPBF can be drastically reduced by the

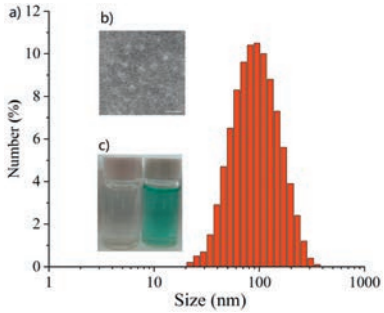

Fig. 3. (a) The diameter of **NBDP-**NPs in aqueous solution detected by DLS. (b) Inset: TEM imaging. Scale bar: 300 nm. (c) Photo of pure water and **NBDP-**NPs in aqueous solution.

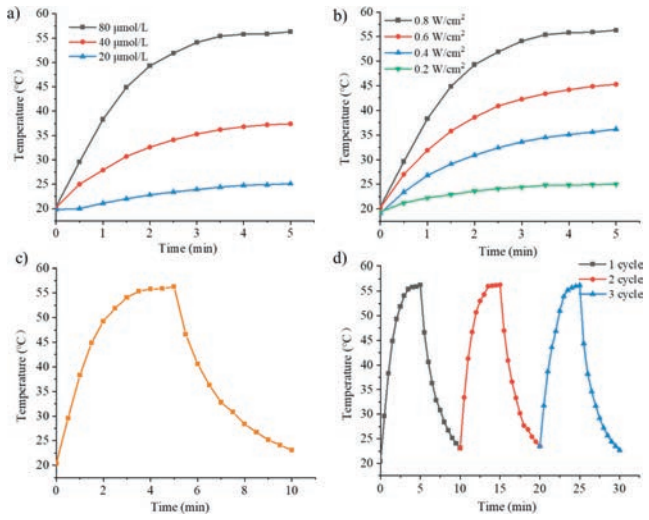

Fig. 4. (a) Photothermal conversion of **NBDP-**NPs at varying concentrations (20–80 μmol/L) was investigated under 690 nm light irradiation (0.8 W/cm^2). (b) Photothermal conversion of 80 μmol/L **NBDP-**NPs under 0.2–0.8 W/cm^2 laser illumination. (c) Photothermal curve of 80 μmol/L **NBDP-**NPs in aqueous media under 0.8 W/cm^2 light exposure and then naturally cooling to ambient temperature. (d) Evaluation of photothermal stability following three cycles of heating and cooling.

interaction of DPBF with $^1O_2$ to form a cyclic compound. Herein, the absorbance of DPBF at 416 nm decreases not obvious decline in presence of **NBDP** than it does in the lack of **NBDP** (Fig. S9a in Supporting information). The absorbance ($\Delta\lambda_{abs}$) of DPBF in toluene containing **NBDP** only decreased by 0.018 after 12 min of light, indicating that the singlet oxygen generation of **NBDP** is entirely negligible under the radiation (Fig. S9b in Supporting information). Whereas, the photostability (λ_{abs} = 678 nm) under illumination is an essential indicator that the dye will not decompose and will present a long-lasting therapeutic effect on the malignancy tumor.

The photothermal conversion of **NBDP-**NPs in aqueous solution was investigated (Fig. 4). After being exposed to light sources, the solution temperature significantly increased. After laser irradiation (690 nm, 0.8 W/cm^2, 5 min) with the corresponding concentration (80 μmol/L) of **NBDP-**NPs, the temperature increment of **NBDP-**NPs (T_{max} = 56.3 °C) was substantially increased. It was discovered that the temperature rises with exposure time, demonstrating that **NBDP-**NPs can convert the optical energy into the thermal energy. The photothermal effect of **NBDP-**NPs was also investigated at concentrations ranging from 20 μmol/L to 80 μmol/L. According to Fig. 4a, the temperature was risen rapidly in the first 2 min, after which, the trend declined and reached a plateau. Also, it was found that **NBDP-**NPs concentration was in responsible of controlling temperature rise (Fig. 4b and Fig. S10 in Supporting information). In addition, the relationship between temperature and laser power density was also investigated. The photothermal effect was associated with the amounts of **NBDP-**NPs as well as the laser exposure intensity and duration, indicating that the degree of temperature rise could be precisely controlled (Figs. 4b and c). Moreover, **NBDP-**NPs demonstrated outstanding thermal stability and photostability under continuous laser illumination, showing no degradation after three cycles of heating and cooling (Fig. 4d). The formula from the experimental approach was subsequently employed to calculate the photothermal conversion efficiency. It was calculated to be approximately 46.9% (Fig. S11 in Supporting information), which was considerably greater than that of previously recorded indocyanine green (ICG) NPs (17.3%), demonstrating that this method of exploring the photothermal conversion by modifying at 1-site in BODIPY system performs effectively.

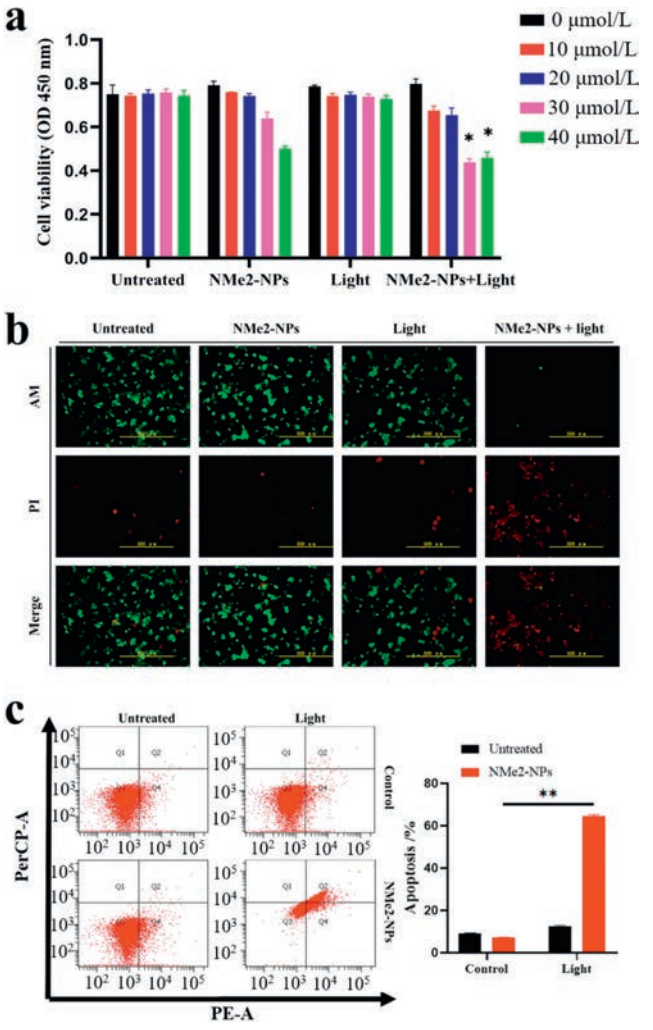

Fig. 5. (a) Cell viability to determine the concentration-dependent effect of **NBDP-**NPs (0–40 μmol/L). (b) Fluorescence images of co-stained AM and PI on after **NBDP-**NPs-treated with or without laser irradiation. Scale bar: 500 μmol/L. (c) Apoptosis analysis after treatment with **NBDP-**NPs alone, light alone, or their combination. Light irradiation (0.3 W/cm^2, 20 min) and 30 μmol/L **NBDP-**NPs was applied. $^*P < 0.05$, $^{**}P < 0.01$ compared with control group. The error bars ($n = 3$) represent mean ± standard deviation (SD). For clarity, **NBDP-**NPs are abbreviated as NMe2-NPs in Fig. 5.

Human colorectal cancer cells (SW-620) were treated with various **NBDP-**NPs concentrations (0–40 μmol/L) and laser radiation, and the cell counting kit-8 (CCK-8) assessment was utilized to determine the concentration dependency of **NBDP-**NPs. The results revealed that, when compared to the no-treatment group, the **NBDP-**NPs treatment group, and the laser radiation group, the combination of laser radiation and **NBDP-**NPs had the most significant effect on decreasing cell viability. There was **NBDP-**NPs concentration dependence, with the discrepancy increasing more noticeable at **NBDP-**NPs concentrations of 30 μmol/L. As a result, we determined to use 30 μmol/L **NBDP-**NPs in the following studies (Fig. 5a). Live-dead cell labeling with calcein AM (green) and propidium iodide (PI, red) reagents was conducted in order to vividly observe efficiency of the phototherapeutic function of **NBDP-**NPs. The green fluorescence denotes living cells, whereas the red fluorescence reflects dead cells. The red fluorescence following NIR photoexcitation (0.3 W/cm^2, 20 min) proved that 30 μmol/L **NBDP-**NPs severely destroyed the cancer cells (Fig. 5b). Nevertheless, only green fluorescence was detected in the solo light and sole NPs groups, confirming that the combination of **NBDP-**NPs with laser

irradiation significantly promoted cytotoxic effects. Moreover, the intracellular ROS production was performed by DCFH-DA assays to detect using flow cytometry. As shown in Fig. S12 (Supporting information), the intracellular ROS level of **NBDP-**NPs groups treated with light has no significant difference compared to the **NBDP-**NPs groups without light. As shown in Fig. 5c, cells treated with **NBDP-**NPs or light alone displayed lesser rates of apoptosis, the fraction of apoptotic cells increased from 9.3% to 65% after treatment with **NBDP-**NPs and laser irradiation, suggesting the efficacy of **NBDP-**NPs stimulated by illumination in inducing apoptosis in cancer cells, rather than necrosis which can cause increased inflammation for therapeutic side-effect.

In conclusion, **NBDP** PTA by a phenyl[*b*]-fused strategy combined with Knoevenagel condensation at 1-site in BODIPY system was constructed, which by self-assembly serves as nanomaterials to prepare **NBDP-**NPs for photothermal therapy (PTT) *via* apoptosis mechanism. **NBDP-**NPs were found to have NIR absorption, and possessed the outstanding PCE of 46.9%, thereby endowing the nanomaterials with PTT anti-cancer reagent. Herein, the feasible modification of BODIPY supports a meticulous-design molecular structure, which can not only achieve innovative molecule construction, but also undertake anti-tumor PTT treatment *via* apoptosis mechanism, rather than necrosis caused increased inflammation for therapeutic side-effect.

Declaration of competing interest

The authors declare that they have no known competing financial interests or personal relationships that could have appeared to influence the work reported in this paper.

Acknowledgments

This work was supported by the National Natural Science Foundation of China (Nos. 22078201, U1908202), Natural Science Foundation of Liaoning (No. 2021NLTS1206), “Chunhui Program” cooperative research project of Education Ministry, Liaoning & Shenyang Key Laboratory of Functional Dye and Pigment (Nos. 2021JH13/10200018, 21–104–0–23). We thank Dr. Rong Shang (Hiroshima University) for the help.

Supplementary materials

Supplementary material associated with this article can be found, in the online version, at doi:10.1016/j.cclet.2023.108862.

References

[1] J. Wang, C. Yu, E. Hao, et al., Coord. Chem. Rev. 470 (2022) 214709.
[2] Y. Wang, D. Zhang, K. Xiong, et al., Chin. Chem. Lett. 33 (2022) 115–122.
[3] J. Wang, N. Boens, L. Jiao, et al., Org. Biomol. Chem. 18 (2020) 4135–4156.
[4] A. Loudet, K. Burgess, Chem. Rev. 107 (2007) 4891–4932.
[5] H. Lu, J. Mack, Z. Shen, et al., Chem. Soc. Rev. 43 (2014) 4778–4823.
[6] Q. Gong, Y. Xiao, E. Hao, et al., J. Am. Chem. Soc. 144 (2022) 21992–21999.
[7] W. Miao, E. Hao, L. Jiao, et al., Chem. Eur. J. 29 (2023) e202203832.
[8] W. Sheng, Z. Wang, E. Hao, L. Jiao, Chin. Chem. Lett. 32 (2021) 1249–1252.
[9] R. Wang, J. Chen, C. Zhao, et al., Chem. Sci. 10 (2019) 7222–7227.
[10] H. Zhang, J. Liu, W. Guo, et al., J. Am. Chem. Soc. 142 (2020) 17069–17078.
[11] L. Gai, Y. Liu, H. Lu, et al., Coord. Chem. Rev. 481 (2023) 215041.
[12] A. Aguiar, J. Farinhas, W. Silva, et al., Dyes Pigment. 172 (2020) 107842.
[13] A. Aguiar, J. Farinhas, W. Silv, et al., Dyes Pigment. 193 (2021) 109517.
[14] D. Tungulin, J. Leier, A.B. Carter, et al., Chem. Eur. J. 25 (2019) 3816–3827.
[15] M. Chapran, E. Angioni, N.J. Findlay, et al., ACS Appl. Mater. Interfaces 9 (2017) 4750–4757.
[16] J. Zou, L. Li, X. Chen, et al., Adv. Mater. 33 (2021) 2103627.
[17] Z. Wang, L. Huang, Y. Yan, et al., Angew. Chem. Int. Ed. 59 (2020) 16114–16121.
[18] D. Chen, Q. Yu, X. Dong, et al., Small 16 (2020) 2001059.
[19] K.X. Teng, L.Y. Niu, Q.Z. Yang, J. Am. Chem. Soc. 145 (2023) 4081–4087.
[20] D. Xi, M. Xiao, X. Peng, et al., Adv. Mater. 32 (2020) 1907855.
[21] H. Dang, D. Yin, Y. Tian, et al., J. Mater. Chem. B 10 (2022) 5279–5290.
[22] C. Ma, T. Zhang, Z. Xie, J. Mater. Chem. B 9 (2021) 7318–7327.
[23] T. Zhang, X. Ma, H. Tian, Chem. Sci. 11 (2020) 482–487.
[24] P. Rana, N. Singh, P. Majumdar, et al., Coord. Chem. Rev. 470 (2022) 214698.
[25] J. Zhao, K. Xu, W. Yang, et al., Chem. Soc. Rev. 44 (2015) 8904–8939.
[26] T. Yu, D. Zhang, X.D. Jiang, et al., J. Mater. Chem. B 10 (2022) 3048–3054.
[27] D. Zhang, N. Xu, X. Peng, et al., Chin. J. Chem. 36 (2018) 119–123.
[28] L. Gai, J. Mack, H. Yamada, et al., Chem. Eur. J. 20 (2014) 1091–1102.
[29] R. Hu, M. Hassan, L. Liu, S. Zhang, W. Gong, Chin. Chem. Lett. 34 (2023) 107541.
[30] X. Jiang, S. Yue, K. Chen, et al., Chin. Chem. Lett. 30 (2019) 2271–2273.
[31] J. Li, Y. Dong, Y. Yang, et al., J. Am. Chem. Soc. 144 (2022) 14351–14562.
[32] Z. Ye, C. Xiong, J. Pan, et al., Dyes Pigment. 155 (2018) 30–35.
[33] X. Zhang, L. Chen, Y. Xiao, et al., Chem. Eur. J. 27 (2021) 3688–3693.
[34] P. Xiao, Z. Shen, B.Z. Tang, et al., Adv. Sci. 9 (2022) 2104079.
[35] M. Tian, D. Guo, W. Lin, Dyes Pigm. 197 (2022) 109951.
[36] K. Li, X. Duan, Z. Jiang, et al., Nat. Commun. 12 (2021) 2376.
[37] L. Zeng, T. Chen, J.S. Kim, et al., Chem. Sci. 13 (2022) 4523–4532.
[38] Z. Ye, M. Ji, D. Liu, et al., Angew. Chem. Int. Ed. 61 (2022) e202204518.
[39] Y. Liu, P. Bhattarai, X. Chen, et al., Chem. Soc. Rev. 48 (2019) 2053–2108.
[40] Q. Yu, L. Tu, Q. Zhao, et al., ACS Appl. Mater. Interfaces 14 (2022) 50637–50648.
[41] J.R. Melamed, R.S. Edelstein, E.S. Day, ACS Nano 9 (2015) 6–11.
[42] M.P. Hernandez, P.D. Pino, S.G. Mitchell, et al., ACS Nano 9 (2015) 52–61.